

# The Pacific-Indian Ocean Associated Mode in CMIP5

## Models

Minghao Yang, Xin Li\*, Weilai Shi, Chao Zhang, Jianqi Zhang

College of Meteorology and Oceanography, National University of Defense Technology, Nanjing, 211101, China

*Correspondence to:* Xin Li (lixin\_atocean@sina.cn)

**Abstract.** The Pacific-Indian Ocean associated mode (PIOAM), defined as the first dominant mode (empirical orthogonal function, EOF1) of SST anomalies in the Pacific-Indian Ocean between 20°S and 20°N, is the product of the tropical air-sea interaction at the cross-basin scale and the main mode of ocean variation in the tropics. Evaluating the capability of current climate models to simulate the PIOAM and finding the possible factors that affect the simulation results are beneficial to obtain more accurate future climate change prediction. Based on 55-yr the Hadley Centre Global Sea Ice and Sea Surface Temperature (HadISST) dataset and the output data from twenty-one Coupled Model Intercomparison Project (CMIP) phase 5 (CMIP5) models, the PIOAM in these CMIP5 models is assessed. Instead of using the time coefficient (PC1) of the PIOAM as its index, we chose to utilize the alternative PIOAM index (PIOAMI), defined with sea surface temperature anomaly (SSTA) differences in the boxes, to describe the PIOAM. It is found that the explained variance of PIOAM in almost all twenty-one CMIP5 models are underestimated. Although all models reproduce the spatial pattern of the positive sea surface temperature anomaly in the eastern equatorial Pacific well, only one-third of these models successfully simulate the ENSO mode with the east-west inverse phase in the Pacific Ocean. In general, CCSM4, GFDL-ESM2M and CMCC-CMS have a stronger capability to capture the PIOAM than that of the other models. The strengths of the PIOAM in the positive phase in less than one-fifth of the models are slightly stronger, and very close to HadISST dataset, especially in CCSM4. The interannual variation of PIOAM can be measured by CCSM4, GISS-E2-R and FGOALS-s2.

## 1. Introduction

As early as the 1960s, Bjerkness (1966, 1969) studied the phenomenon of El Niño-Southern Oscillation (ENSO). Since then, the impact of ENSO on global climate has become a major concern in

32 climate research. ENSO in the Pacific Ocean is the strongest interannual signal of global climate change,  
33 and has been extensively studied by a large number of scholars, including its occurrence and development  
34 mechanism (Wyrтки, 1975; Philander et al., 1984; Suarez and Schopf, 1988; Jin, 1997; Li and Mu, 1999;  
35 Li and Mu, 2000; Li, 2002), its evolution characteristics and its impact on global weather and climate  
36 (Bjerknes, 1966; Rasmusson and Wallace, 1983; Ropelewski and Halpert, 1987; Li, 1990; Webster and  
37 Yang, 1992; Zhou and Zeng, 2001; Mu and Duan, 2003; Mu et al., 2007; Zheng et al., 2007). At the end  
38 of the 20th century, an interannual climate anomaly characterized by a sea surface temperature anomaly  
39 (SSTA) of opposing sign in the western and eastern tropical Indian Ocean, known as the Indian Ocean  
40 dipole (IOD), was reported by Saji et al. (1999) and Webster et al. (1999) and was catalogued as one of  
41 the major ocean-atmosphere coupled phenomena. The SSTA in the tropical Indian Ocean subsequently  
42 has been widely studied, and a great deal of literature has discussed the causes and mechanisms of the  
43 IOD, as well as its weather and climate impacts (Li and Mu, 2001; Li et al., 2003; Saji and Yamagata,  
44 2003; Cai et al., 2005; Rao et al., 2007; Zheng et al., 2013; Wang and Wang, 2014).

45 IOD was initially thought to be generated only by independent air-sea interactions in the tropical  
46 Indian Ocean, but some studies have suggested that the tropical Indian Ocean SSTA in 1997/1998 was  
47 caused by the influence of the ENSO event in the Pacific Ocean on the surface wind field of the Indian  
48 Ocean through anti-Walker circulation over the equator, thus causing the SSTA in the Indian Ocean (Yu  
49 and Rienecker, 1999). It has also been suggested that the east-west asymmetry anomaly of the Indian  
50 Ocean SSTA in 1997/1998 may contain the triggering process of ENSO (Ueda and Matsumoto, 2000).  
51 Li et al. (2002) showed that there is a significant negative correlation between the tropical Indian Ocean  
52 SSTA dipole event and the Pacific SSTA dipole event (similar to ENSO mode) using statistical analysis.  
53 Huang and Kinter (2002) also noted that there was a significant relationship between IOD in the Indian  
54 Ocean and ENSO in the Pacific Ocean.

55 The movements and changes of Earth's fluids (atmosphere and oceans) have a certain connection,  
56 and the change in tropical sea surface temperature (SST) should not be an isolated phenomenon. IOD in  
57 the Indian Ocean and ENSO in the Pacific Ocean, both as significant basin-scale signals, are supposed  
58 to be closely related and interact with each other. Although the type of relationship between ENSO and  
59 IOD has not yet been fully demonstrated, extensive research has shown that both SST and the air-sea  
60 systems in the Pacific Ocean and the Indian Ocean are closely linked (Klein and Soden, 1999; Li et al.,

61 2008; Huang and Kinter, 2002; Li et al., 2003; Annamalai et al., 2005; Cai et al., 2019). The Walker  
62 circulation anomaly induced by SSTA over the equatorial Pacific Ocean will cause a Walker circulation  
63 anomaly over the Indian Ocean, which could inspire the occurrence and development of IOD in the  
64 Indian Ocean driven by abnormal wind stress in the lower layer. On the other hand, Indonesian  
65 Throughflow also plays a role in the connection between ENSO and IOD. The cold (El Nino) or warm  
66 (La Nina) SST of the warm pool in the Pacific Ocean can cool or warm the SST in the eastern equatorial  
67 Indian Ocean through the Indonesian Throughflow, which is conducive to the establishment of a positive  
68 or negative phase of IOD.

69 Yang and Li (2005) found the first leading mode of the tropical Pacific-Indian SSTA reflecting the  
70 opposite phase characteristics of both the middle west Indian Ocean and equatorial middle east Pacific  
71 Ocean and both the eastern Indian Ocean and equatorial western Pacific Ocean, from which they  
72 proposed the concept of the Pacific-Indian Ocean associated mode (PIOAM), and noted that the PIOAM  
73 can better reflect the influence of the tropical SSTA on Asian atmospheric circulation. Yang et al. (2006)  
74 subsequently found that the influences of the PIOAM and the ENSO mode on summer precipitation and  
75 climate in China were very different, and their numerical experiments also showed that the simulation  
76 results obtained by considering the PIOAM were more consistent with observation data. Based on multi-  
77 variable empirical orthogonal functions, Chen and Cane (2008) and Chen (2011) also found this  
78 phenomenon and named it Indo-Pacific Tripole (IPT), which is considered to be an intrinsic mode in the  
79 tropical Indo-Pacific Ocean. In addition, Lian et al. (2014) used a conceptual model to discuss the  
80 development and physical mechanism of the IPT. By analyzing the monthly thermocline temperature  
81 anomaly (TOTA) from 1958-2007 and the weekly sea surface height (SSH) anomaly from 1992-2011 in  
82 the tropical Pacific-Indian Ocean, Li et al. (2013) further found that the PIOAM are more obviously in  
83 the subsurface ocean temperature anomaly field, especially in the thermocline. Based on the simulation  
84 results of the LASG/IAP (State Key Laboratory of Numerical Modeling for Atmospheric Sciences and  
85 Geophysical Fluid Dynamics/Institute of Atmospheric Physics) Climate system Ocean Model (LICOM),  
86 version 2 (LICOM2.0) (Liu et al. 2012) and observation data, Li and Li (2017) proved that PIOAM is an  
87 important tropical Pacific-Indian Ocean SST variation mode that actually exists both in observation and  
88 simulation. Therefore, when studying the influence of SSTA in the Pacific and Indian oceans on weather  
89 and climate, the Pacific and Indian oceans should be considered as unified.

90 Since the PIOAM is so important, how well do current climate models simulate it? To answer this  
 91 question, the outputs from the climate system models for the Coupled Model Intercomparison Project  
 92 (CMIP) phase 5 (CMIP5) were used for this research, from which we aim to provide a more complete  
 93 evaluation of the PIOAM and try to find possible reasons that cause the simulation biases. In the  
 94 following, Sect. 2 includes a brief description of the HadISST dataset, CMIP5 models, and the methods  
 95 used in this study. Section 3 presents the assessments of the PIOAM in the CMIP5 models. A conclusion  
 96 and discussion are given in Sect. 4.

97

98 **2. Data and methods**

99

100 The SST data from the Hadley Centre Global Sea Ice and Sea Surface Temperature (HadISST)  
 101 (Rayner et al., 2003) dataset is used for this study. The data are monthly averaged data from 1951 to 2005  
 102 with a spatial resolution of  $1^\circ \times 1^\circ$ . Brief information for the 21 CMIP5 models for the historical period  
 103 used in this article is provided in Table 1. It's worth noting that some models have higher resolution in  
 104 tropics. Considering that output data resolutions vary between the models, we first interpolated all data  
 105 into a  $1^\circ \times 1^\circ$  grid to facilitate comparison between the models and HadISST dataset.

106

107

Table 1. List of 21 selected CMIP5 climate models.

Model name	Modeling group	Oceanic resolution (lon×lat)
CanESM2 (Second Generation Canadian Earth System Model)	Canadian Centre for Climate Modeling and Analysis, Canada	256×192
CCSM4 (The Community Climate System Model, version 4)	NCAR, USA	320×384
CMCC-CESM (Centro Euro-Mediterraneo sui Cambiamenti Climatici (CMCC) Carbon Earth System Model)	CMCC, Italy	182×149
CMCC-CM (CMCC Climate Model)	CMCC, Italy	182×149
CMCC-CMS (CMCC-CM with a resolved stratosphere)	CMCC, Italy	182×149
CNRM-CM5 (Centre National de Recherches Météorologiques (CNRM) Coupled Global Climate Model, version 5)	CNRM, France	362×292
FGOALS-s2 (The Flexible Global Ocean-Atmosphere-Land System model, Spectral Version 2)	LASG, China	360×196
GFDL-ESM2M (Earth System Model of Geophysical Fluid Dynamics Laboratory (GFDL) with Modular Ocean Model, version 4)	GFDL, USA	144×90
GISS-E2-H (Goddard Institute for Space Studies (GISS) Model E version 2 (GISS-E2) with HYCOM ocean model)	NASA, USA	144×90
GISS-E2-H-CC (GISS-E2-H with carbon cycle)	NASA, USA	144×90
GISS-E2-R (GISS-E2 with Russell ocean model)	NASA, USA	144×90
GISS-E2-R-CC (GISS-E2-R with carbon cycle)	NASA, USA	144×90
HadCM3 (the third version of the Hadley Centre coupled model)	Met Office Hadley Centre, UK	288×144

HadGEM2-AO (Hadley Global Environment Model 2 (HadGEM2)- Atmosphere-Ocean)	Met Office Hadley Centre, UK	360×216
HadGEM2-CC (HadGEM2-Carbon Cycle)	Met Office Hadley Centre, UK	360×216
HadGEM2-ES (HadGEM2-Earth System)	Met Office Hadley Centre, UK	360×216
IPSL-CM5B-LR (Institut Pierre Simon Laplace Climate Model 5B (LPSL-CM5B)-Low Resolution)	IPSL, France	182×149
IPSL-CM5B-MR (LPSL-CM5B 5A-Medium Resolution)	IPSL, France	182×149
MIROC-ESM (Model for Interdisciplinary Research on Climate, Earth System Model)	Atmosphere and Ocean Research Institute (AORI), Japan	256×192
MIROC-ESM-CHEM (An atmospheric chemistry coupled version of MIROC-ESM)	AORI, Japan	256×192
NorESM1-M (Norwegian Climate Centre Earth System Model)	Norwegian Climate Centre, Norway	384×320

108

109 The PIOAM is determined according to the method of Ju et al. (2004) and Li et al. (2018), that is,  
110 the first leading mode (empirical orthogonal function, EOF1) of the tropical Pacific-Indian ocean  
111 SSTA (20°S-20°N, 40°E-80°W) is used to represent the PIOAM. The annual cycle and the linear trend  
112 are removed to obtain the monthly SSTA. Ju et al. (2004) used this method to analyze SSTA in the tropical  
113 Pacific-Indian Ocean in different seasons, and found the existence of PIOAM in all seasons with a  
114 contribution to total variance of more than 33%, indicating that the spatial distribution structure of  
115 PIOAM was stable.

116 Accounting for the intimate connection between the Pacific ENSO mode and the Indian Ocean  
117 dipole, Yang et al. (2006) argued that the PIOAM index (PIOAMI) can be defined as the respectively  
118 normalized east-west SSTA differences of the equatorial areas in the two oceans. As to the SSTA, the  
119 SSTA of ENSO is stronger than that in the equatorial Indian Ocean because of the larger Pacific basin;  
120 however, as to the influence of the SSTA on East Asia, a series of numerical experiments clearly indicate  
121 that the effect of SSTA forcing on the Indian Ocean is stronger than that of the eastern equatorial Pacific  
122 (Shen et al., 2001; Guo et al., 2002; Guo et al., 2004; Yang et al., 2006). Therefore, the PIOAMI is  
123 defined on the basis of the respective normalized dipoles in the Pacific and the Indian Ocean. According  
124 to the method of Yang et al. (2006), The PIOAMI is defined as follows:

125 
$$\text{PIOAMI} = \text{IOI} + \text{POI} \quad (1)$$

126 
$$\text{IOI} = \text{SSTA}(5^{\circ}\text{S} - 10^{\circ}\text{N}, 50^{\circ}\text{E} - 65^{\circ}\text{E}) - \text{SSTA}(10^{\circ}\text{S} - 5^{\circ}\text{N}, 85^{\circ}\text{E} - 100^{\circ}\text{E}) \quad (2)$$

127 
$$\text{POI} = \text{SSTA}(5^{\circ}\text{S} - 5^{\circ}\text{N}, 130^{\circ}\text{W} - 80^{\circ}\text{W}) - \text{SSTA}(5^{\circ}\text{S} - 10^{\circ}\text{N}, 140^{\circ}\text{E} - 160^{\circ}\text{E}) \quad (3)$$

128 where IOI and POI are the normalized Indian Ocean and Pacific Ocean indices, respectively.

129

### 130 3. Results

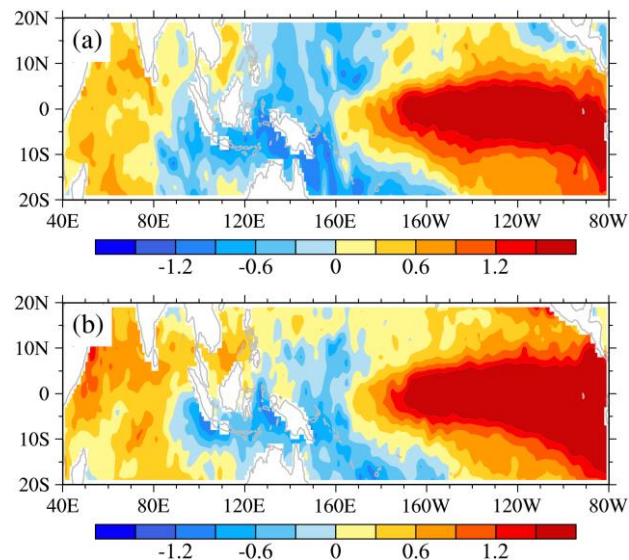
131

#### 132 3.1 Spatial pattern

133

134 Figure 1 shows the pattern of SST anomalies over the Indo-Pacific Ocean in October 1982 and  
135 September 1997. It can be clearly seen that there are obvious warm tongues in the eastern equatorial  
136 Pacific Ocean, obvious positive SST anomalies in the northwest Indian Ocean, and obvious negative SST  
137 anomalies in the western equatorial Pacific Ocean and the eastern Indian Ocean. This is precisely the  
138 typical spatial pattern characteristics of the PIOAM mentioned above. That is to say, the SST anomalies  
139 in the northwest Indian Ocean and the equatorial middle-east Pacific Ocean is opposite to the SST  
140 anomalies in the western equatorial Pacific Ocean and the east Indian Ocean. Compared with ENSO and  
141 IOD, the PIOAM has a broader spatial distribution.

142



143

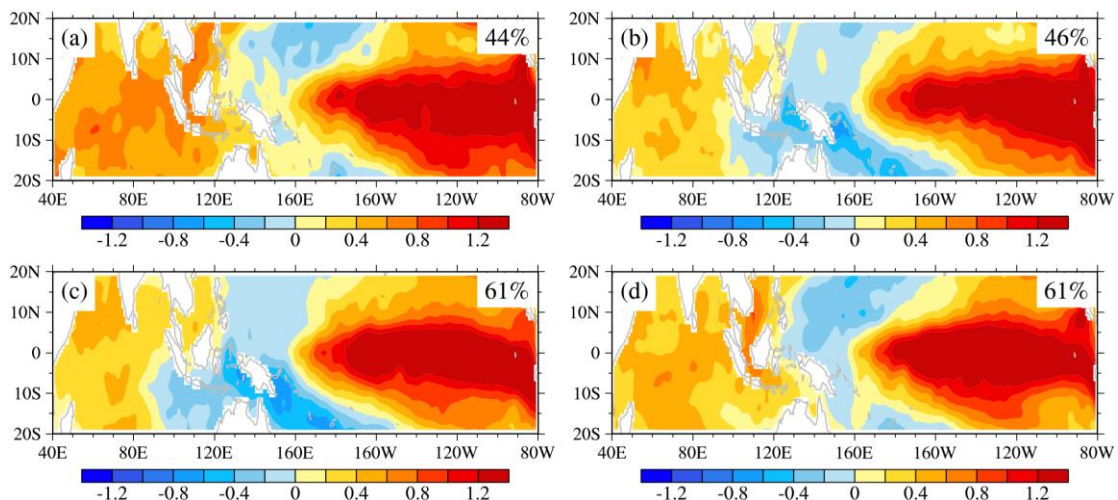
144 **Figure 1: Maps of SST anomalies for (a) October 1982 and (b) September 1997 from the HadISST dataset**  
145 **(unit: °C). The period from 1981 to 2005 is used to extract the monthly SST climatology.**

146

147 However, is this spatial pattern of SST anomalies only a special case of a certain year, or is it stable?  
148 To answer this question, EOF analysis is performed on the SST anomalies of different seasons over Indo-  
149 Pacific Ocean (20°S-20°N, 40°E-80W°) from 1951 to 2005. All these first leading modes in Fig. 2 are  
150 well separated from the remaining leading modes, based on the criteria of North et al. (1982), which

151 means less likely to be affected by statistical sampling errors. It can be found that the patterns of summer  
 152 (June, July and August; Fig. 2.b) and autumn (September, October and November; Fig. 2.c) display the  
 153 typical spatial distribution of the PIOAM, with the 46% and 61% contribution to total variance,  
 154 respectively, while the spatial pattern of PIOAM is not so obvious in spring (March, April and May; Fig.  
 155 2.a) and winter (December, January and February; Fig. 2.d). In general, the PIOAM has stable structure  
 156 and practical significance, especially in autumn.

157



158

159 **Figure 2: Spatial patterns of the first leading mode of the (a) spring (March, April and May), (b) summer**  
 160 **(June, July and August), (c) autumn (September, October and November) and (d) winter (December, January**  
 161 **and February) averaged SST anomalies over Indo-Pacific Ocean (20°S-20°N, 40°E-80°W) calculated from**  
 162 **HadISST dataset (unit: °C). The numbers at the upper right corner of each panel indicate the percentage of**  
 163 **variance explained by each season.**

164

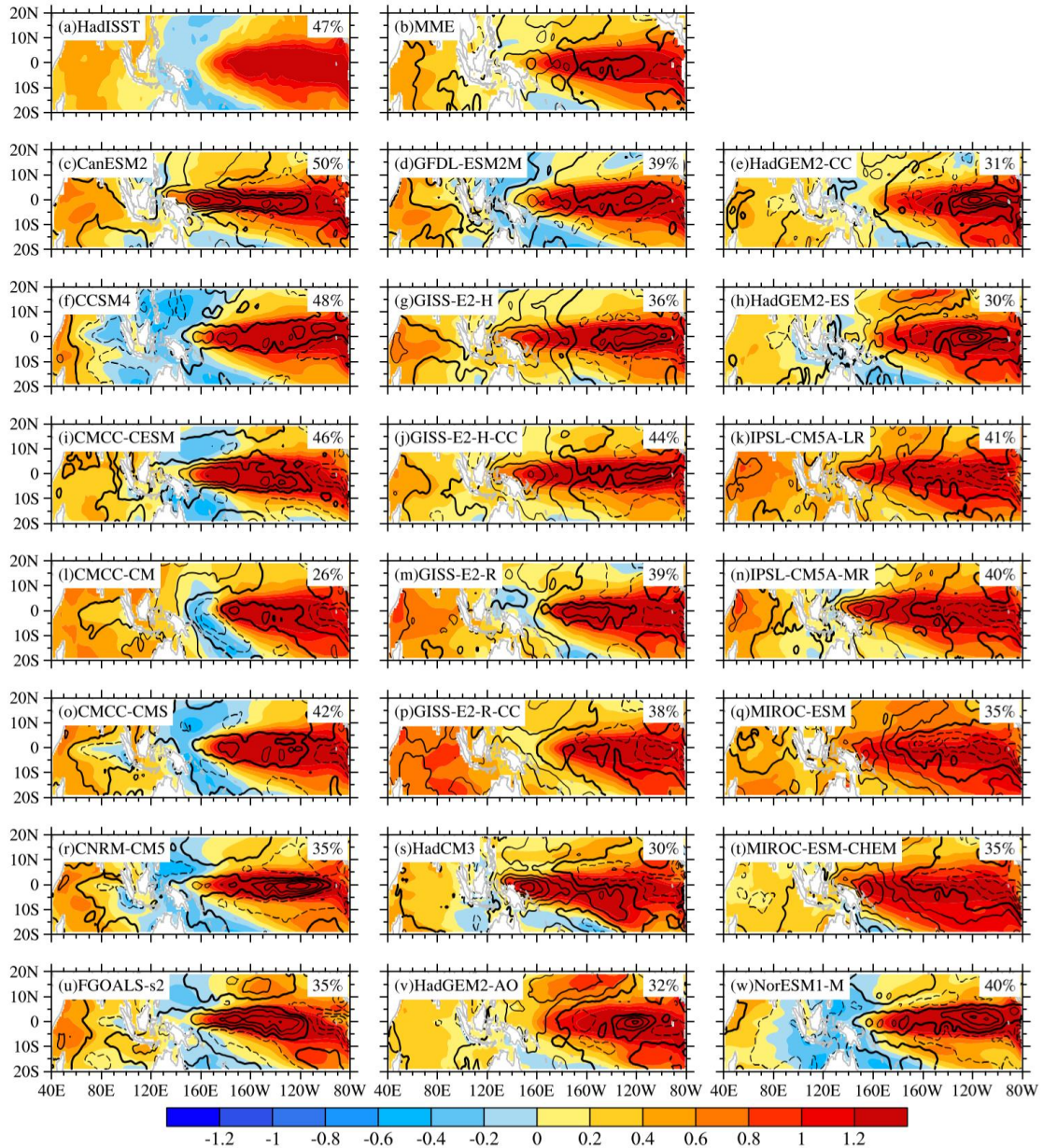
165 Performing the EOF analysis on the monthly SST anomalies regardless of seasonal differences,  
 166 Figure 3 depicts the spatial pattern of PIOAM in the selected 21 CMIP5 models and their differences  
 167 compared to HadISST dataset (Fig. 3a). Figure 3.b shows the results of a multi-model ensemble (MME)  
 168 that represents the mean of the results from all selected models. The PIOAM in HadISST dataset and  
 169 CMIP5 models is well separated from the second leading mode, according to the criterion of North et al.  
 170 (1982). To better and objectively evaluate the capability of each model in simulating PIOAM, a Taylor  
 171 diagram (Fig. 4) is also adopted to concisely display the relative information from multiple models, so  
 172 that the differences among the simulations from all models are revealed clearly (Taylor, 2001; Jiang and  
 173 Tian, 2013; Yang et al., 2018). According to HadISST dataset (Fig. 3.a), with a 47% contribution to total  
 174 variance, the PIOAM has a warm tongue spatial pattern in the eastern equatorial Pacific Ocean, whereas

175 there is negative SSTA in the western equatorial Pacific Ocean, which exhibits an obvious ENSO mode  
176 in the Pacific Ocean. In addition, there are obvious positive SSTA in the western Indian Ocean region of  
177 the PIOAM, but the SSTA in the eastern equatorial Indian Ocean region remain positive. Considering  
178 that the IOD is defined by the difference between the SSTA in the western equatorial Indian Ocean and  
179 that in the eastern equatorial Indian Ocean, this indicates zonal surface heat contrast of the Indian Ocean  
180 SSTA. Although it is called a dipole, it is also like a meridional seesaw (Li et al., 2002; Yang et al., 2006).  
181 Therefore, it can be considered that the PIOAM represents an IOD mode in the Indian Ocean region.

182 Figure 3 shows that all of these models can generally reproduce the spatial pattern of PIOAM, yet  
183 large discrepancies exist regarding the strength, and the differences between the models are also  
184 significant. Except for the contribution to total variance of PIOAM in CCSM4 and CMCC-CESM are  
185 nearly consistent with HadISST dataset, the variance contribution of PIOAM in almost all CMIP5 models  
186 are lower than those in the HadISST dataset, especially CMCC-CM with a contribution to total variance  
187 as small as 26%. In terms of strength, it is apparent that the simulation errors of these models are mainly  
188 concentrated in the Pacific Ocean compared to the Indian Ocean. Compared to the HadISST dataset, a  
189 majority of models overestimate the strength of PIOAM in the equatorial east Pacific and central Pacific;  
190 only one-seventh of the models (IPSL-CM5A-LR, IPSL-CM5A-MR and MIROC-ESM) underestimate  
191 the strength of PIOAM in the equatorial east Pacific, while the simulation results of HadGEM2-AO and  
192 CMCC-CM in the equatorial central Pacific and western Pacific are weak. The simulation errors of the  
193 strength of the ENSO-like mode in CCSM4, CMCC-CMS, GFDL-ESM2M and GISS-E2-R-CC are  
194 lower than those in other models. For the Indian Ocean, the strengths of PIOAM in only approximately  
195 one-quarter of the models (CanESM2, CMCC-CESM, GISS-E2-H-CC, HadCM3 and HadGEM2-AO)  
196 are basically consistent with HadISST dataset with small simulation errors. Nearly half of the models  
197 were smaller for the eastern Indian Ocean, whereas more than half were larger for the western Indian  
198 Ocean. In general, the simulation error in the Indian Ocean region is significantly smaller than that in the  
199 Pacific region. According to Fig. 4, it is apparent that the root mean square errors (RMSEs) in MIROC-  
200 ESM-CHEM, IPSL-CM5A-LR and MIROC-ESM are relatively large, which means that the capabilities  
201 of these modes to simulate the strength of PIOAM are still inadequate, whereas the RMSEs in CCSM4,  
202 CMCC-CMS and GFDL-ESM2M are smaller than in other models with a better performance. In addition,  
203 as shown in Fig. 3.b, MME better simulates the amplitude of PIOAM in the Indian Ocean than most



204 these selected CMIP5 models with smaller simulation errors, but the amplitude in the equatorial Pacific  
 205 are larger than that of the HadISST dataset.  
 206



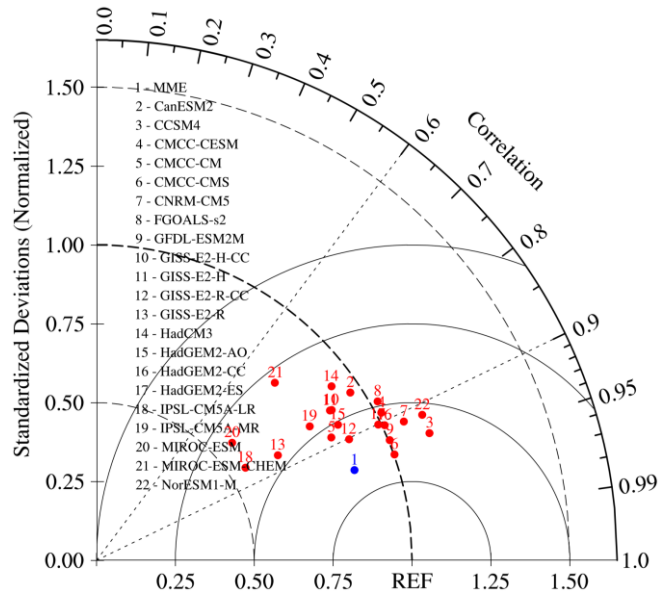
207  
 208 **Figure 3: PIOAM (shading) and the difference between each model and HadISST dataset (contour, with an**  
 209 **interval of 0.3, shown as black bold lines represent the contour with the zero value, dashed contours denote**  
 210 **negative values, unit: °C). The numbers at the upper right corner of each panel indicate the percentage of**  
 211 **variance explained by each model.**  
 212

213 As for spatial patterns, the IOD-like mode in the Indian Ocean region can be simulated in almost all  
 214 models except MIROC-ESM-CHEM. Although all these models reproduce the spatial pattern of the  
 215 positive SSTA well in the eastern equatorial Pacific, only one-third of the models (CCSM4, CMCC-CM,

216 CMCC-CMS, CNRM-CM5, FGOALS-s2, GFDL-ESM2M and NorESM1-M) successfully simulate the  
217 ENSO-like mode with the east-west inverse phase in the Pacific Ocean. In addition, the simulated  
218 positive SSTAs in the eastern equatorial Pacific in HadCM3 and MIROC-ESM-CHEM are further south.  
219 According to Fig. 4, more than one-third of these models (CCSM4, CMCC-CMS and GFDL-ESM2M,  
220 etc.) can simulate the spatial pattern of PIOAM well, and the spatial correlation coefficients between  
221 these models and the HadISST dataset are all greater than 0.9, especially CCSM4, which is as high as  
222 0.95. In contrast, the spatial pattern of PIOAM in MIROC-ESM-CHEM is unsatisfactory with a spatial  
223 correlation coefficient of only 0.69. The simulation results of HadCM3 and MIROC-ESM are also  
224 relatively poor, and the spatial correlation coefficients with HadISST dataset are less than 0.8. It can also  
225 be learned from Fig. 4 that, for the standard deviation of PIOAM, very large differences exist among  
226 these models. The standard deviations of PIOAM in IPSL-CM5A-LR, MIROC-ESM and GISS-E2-R-  
227 CC are quite different from those of the HadISST dataset, while the simulation results of CMCC-CMS,  
228 GFDL-ESM2M and HadGEM2-CC are basically close to those of the HadISST dataset and have better  
229 performance. It is noteworthy that the standard deviations of PIOAM in more than half of these models  
230 are smaller than that of the HadISST dataset, and their differences are large. Although the spatial pattern  
231 of PIOAM in MME is closer to the HadISST dataset and the RMSE is smaller than the vast majority of  
232 single models, the standard deviation of PIOAM in MME is smaller than that of the HadISST dataset.

233 In general, CCSM4, GFDL-ESM2M and CMCC-CMS have a stronger ability to simulate the  
234 PIOAM. In addition, although the MME may not be as good as that of a single model in some specific  
235 aspects, overall, considering spatial pattern, standard deviation and RMSE, MME is still superior to most  
236 single models.

237



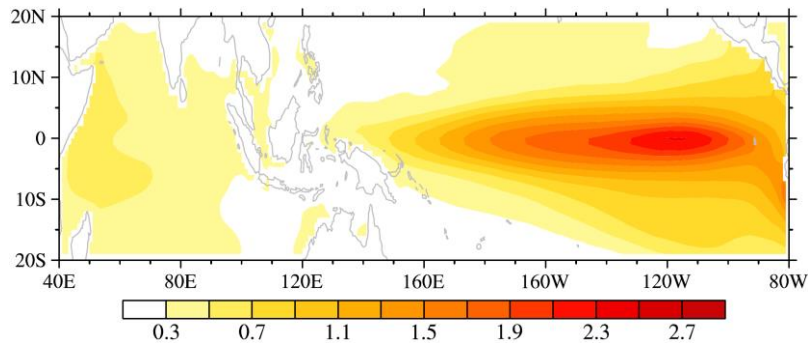
238

239 **Figure 4: Taylor diagram of PIOAM.**

240

241 To further evaluate the differences between these models, Fig. 5 shows the distribution of standard  
 242 deviations between the CMIP5 models, which clearly reflects the regional differences between the  
 243 models. It is apparent that the differences are mainly concentrated in the eastern equatorial Pacific.  
 244 Therefore, the emphasis of improving the model on simulating the PIOAM is to improve the capability  
 245 of the model to simulate to the Eastern-Pacific (EP) type ENSO.

246



247

248 **Figure 5: The standard deviations of simulated PIOAM between the selected 21 CMIP5 models (unit: °C).**

249

### 250 3.2 PIOAM index

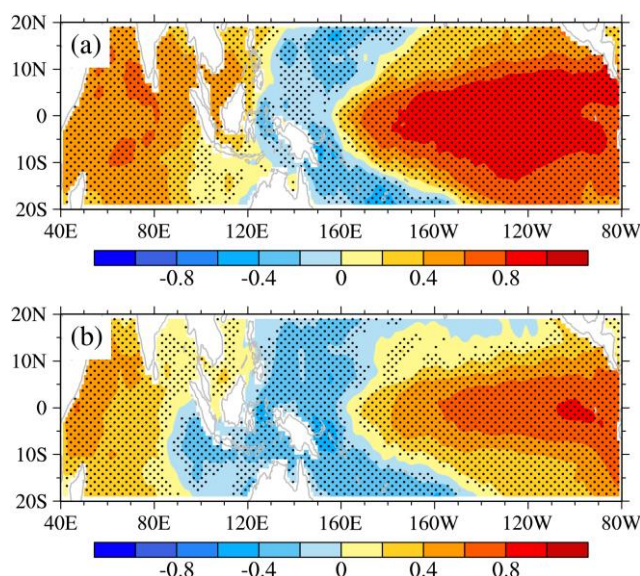
251

#### 252 3.2.1 Time series

253

254 A satisfactory index is needed to describe the PIOAM. It is customary to select the time coefficient  
 255 (PC1) of the PIOAM as its index. It can be seen from the regression of the monthly SSTA onto the

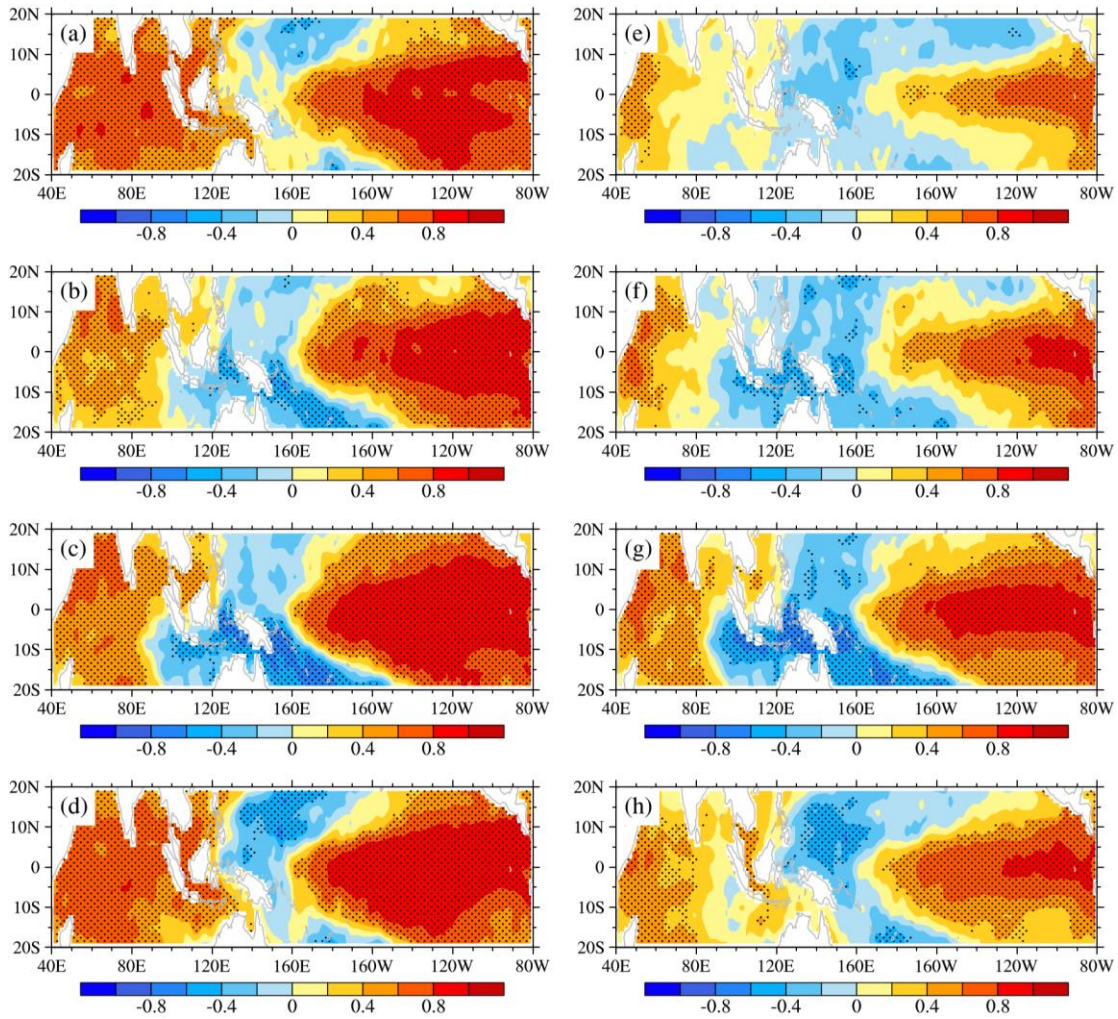
256 normalized PC1 (Fig. 6.a) that the pattern in the Pacific Ocean is similar to ENSO, but positive SST  
 257 anomalies occur throughout the Indian Ocean, which not matches the typical PIOAM spatial pattern.  
 258 This is because the ENSO signals in the Pacific Ocean in PC1 are so strong that the signals of the IOD  
 259 are not fully reflected. The correlation coefficient between PC1 and Niño3.4 index is as high as 0.95.  
 260 However, obvious negative SST anomalies in the eastern Indian Ocean can be found in the regression  
 261 map of the monthly SSTA based on the normalized PIOAMI defined in Section 2. The correlation  
 262 coefficient between PIOAMI and Niño3.4 index is 0.68, indicating PIOAMI contains more Indian Ocean  
 263 signals than PC1. In addition, the correlation coefficient between PC1 and PIOAMI is 0.70, which is far  
 264 more than the confidence level of 99%. Therefore, PIOAMI can describe the mode well because of giving  
 265 consideration to both the signals in the Pacific Ocean and the signals in the Indian Ocean.  
 266  
 267



268  
 269 **Figure 6: Regressions of the monthly SSTA onto the normalized (a) PC1 and (b) PIOAMI for the**  
 270 **period from 1951 to 2005 (unit: °C). The stippled areas for SSTA denote the 99% confidence levels.**  
 271

272 In addition, Figure 7 shows the regressions of the SSTA onto the normalized PC1 and PIOAMI in  
 273 four seasons. It can also be found that the spatial patterns associated with PIOAMI (Fig. 7.e-h) are closer  
 274 to the typical spatial pattern of the PIOAM than that associated with PC1 (Fig. 7.a-d). Although both the  
 275 PC1 and the so-called PIOAMI can describe PIOAM, in the present study, we believe that the PIOAMI  
 276 can better represent the PIOAM than the PC1. Therefore, we chose to only use the PIOAMI to investigate  
 277 the PIOAM in the following studies, instead of using the both indices.





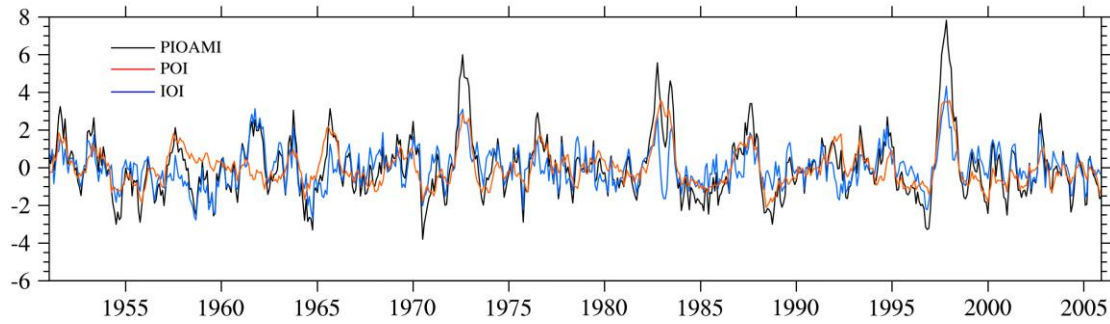
279

280 **Figure 7: Same as Figure 6 but for the regressions of the (a, e) MAM, (b, f) JJA, (c, g) SON and (d,**  
 281 **h) DJF SSTA onto the normalized (a-d) PC1 and (e-h) PIOAMI.**

282

283 Figure 8. shows the monthly time series of the PIOAMI, Pacific Ocean index (POI) and Indian  
 284 Ocean index (IOI) from 1951 to 2005. The wavelet analysis of PIOAMI indicates that PIOAM has  
 285 obvious seasonal and interannual variations, as well as interdecadal variations (feature is omitted).  
 286 According to Fig. 8, POI and IOI have the same variation tendency at most times, thus the PIOAMI  
 287 amplitude is greatly enhanced. However, there are a few cases where the two change in opposing ways,  
 288 resulting in a much weaker PIOAMI. Moreover, from the time-series of PIOAMI, there is an interannual  
 289 oscillation of positive and negative phases in the PIOAM, and there is also a phenomenon that the  
 290 PIOAMI is very weak or not obvious in some years.

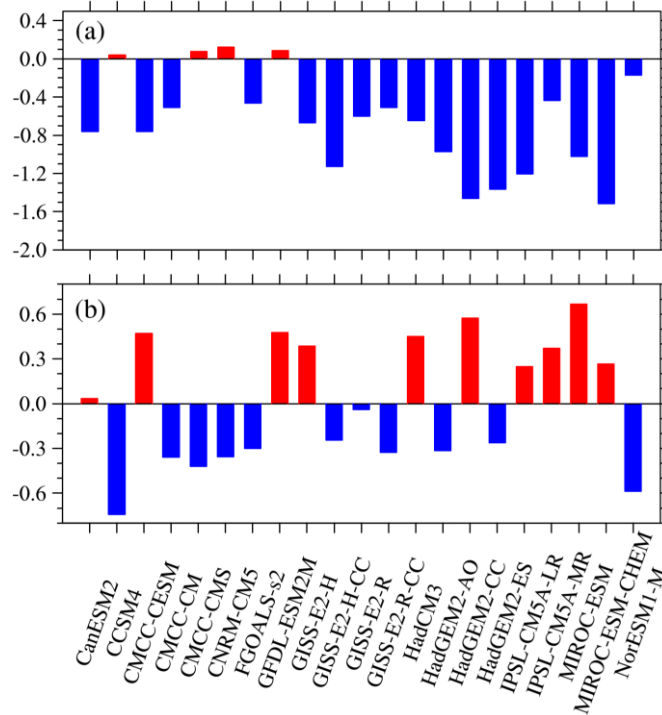
291



292  
 293 **Figure 8: Time-series of PIOAM index (black), Pacific Ocean index (red) and Indian Ocean index (blue) in**  
 294 **the HadISST dataset.**

295  
 296 Considering that the PIOAM mainly reaches its peak in autumn (September, October and  
 297 November), we select the year with significant positive and negative phases of PIOAM by taking one  
 298 standard deviation as the criterion, and calculate the difference of autumn PIOAMI between each CMIP5  
 299 model and the HadISST dataset (see Fig. 9) to further reveal the simulation of the CMIP5 models on the  
 300 strength of the PIOAM. As shown by Fig. 9.a, the simulated strengths of the PIOAM in the positive phase  
 301 are underestimated in most models, whereas they are slightly overestimated in less than one-fifth of the  
 302 models (CCSM4, CMCC-CMS, CNRM-CM5 and GFDL-ESM2M) are slightly stronger, which are very  
 303 close to the HadISST dataset, especially in CCSM4. However, nearly half of the models overestimate the  
 304 strength of the PIOAM in the negative phase (Fig. 9.b), in which the simulation results of CanESM2 and  
 305 GISS-E2-R are consistent with the HadISST dataset. Although CCSM4 has a better performance in  
 306 simulating the strength of the PIOAM in the positive phase than other models, the simulation error of the  
 307 negative phase is very large.

308



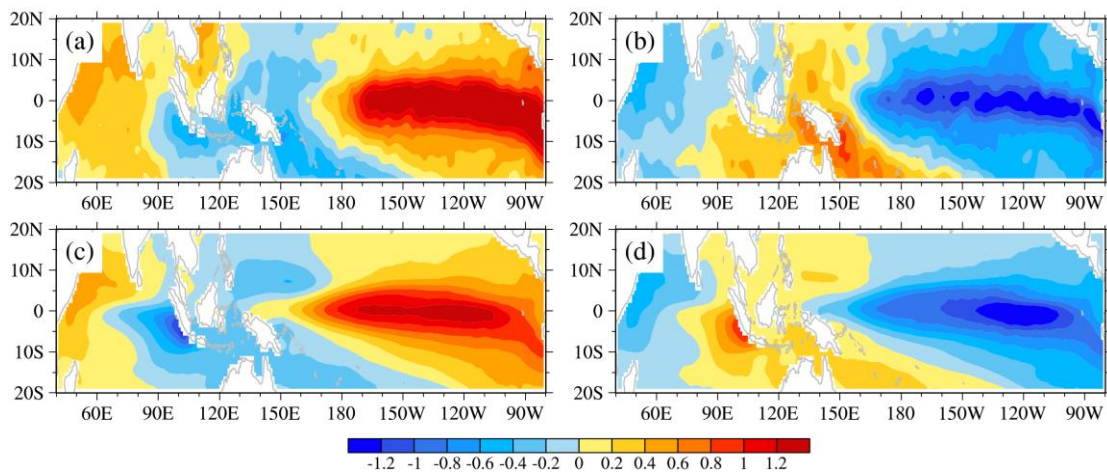
309

310 **Figure 9: Difference in the amplitude of the PIOAMI in the positive phase (a) and negative phase (b) between**  
 311 **the CMIP5 models and HadISST dataset.**

312

313 According to PIOAM positive and negative phase year based on the autumn PIOAMI, SSTAs in  
 314 the tropical Pacific-Indian Ocean in October are composited to obtain the spatial pattern of SSTAs in the  
 315 PIOAM positive and negative phases. It is clear in Fig. 10 that the SSTAs in the Pacific-Indian Ocean in  
 316 both the MME of CMIP5 models and HadISST dataset present patterns with a tripole structure, where  
 317 the Indian Ocean is represented by the IOD-like mode and the Pacific Ocean by the ENSO-like mode,  
 318 which again demonstrates the authenticity of PIOAM and the rationality of PIOAMI used in this article.

319



320

321 **Figure 10: The tropical Pacific-Indian Ocean SSTAs of the PIOAM positive (a, c) and negative (b, d) phase in**

322 **October in the HadISST dataset (a, b) and the MME of CMIP5 models (c, d) (unit: °C).**

323

### 324 3.2.2 Interannual Variation of PIOAM

325

326 To evaluate the ability of these CMIP5 models to simulate the interannual variation of PIOAM, Fig.

327 11 shows the ratios of standard deviation of IOI, POI and PIOAMI in autumn in each model to those in  
328 the HadISST dataset. The closer the ratio is to 1, the better the ability to simulate interannual variation.

329 It can be found that the difference in the simulation results of the interannual variation of PIOAMI among

330 these models is smaller compared to IOI and POI. The simulation results of CCSM4, GISS-E2-R and

331 FGOALS-s2 are almost consistent with HadISST dataset, indicating that these three models have

332 relatively strong capabilities to simulate the interannual variation of PIOAM. Except that NorESM1-M

333 overestimates the interannual variation of PIOAM, the simulation results in most of the models are weak,

334 especially MIROC-ESM, which leads to MME underestimating the interannual variation of PIOAM

335 compared to the HadISST dataset. In addition, the interannual variations of IOI in GFDL-ESM2M, GISS-

336 E2-R-CC and CMCC-CM are better than other models, whereas the simulation results are underestimated

337 in most models. In contrast to IOI, the vast majority of models overestimate the interannual variations of

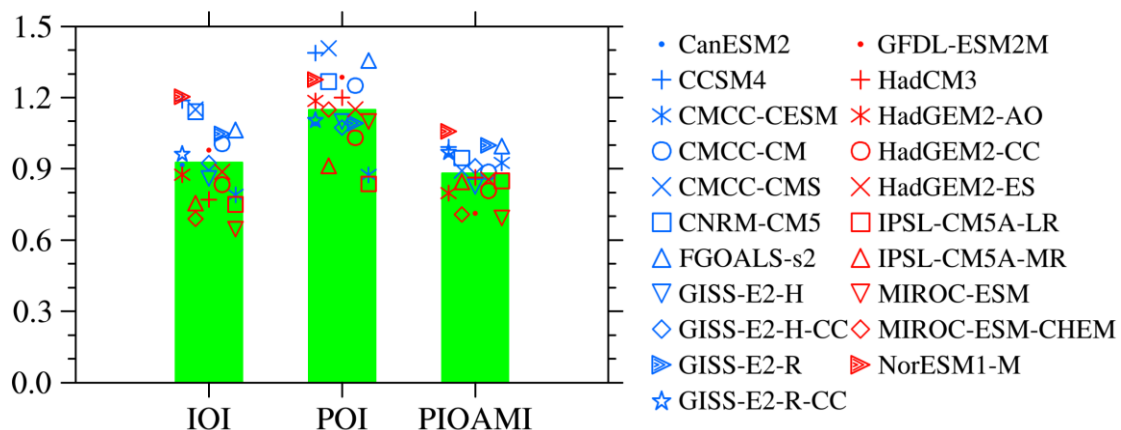
338 POI, and the simulated interannual variations of POI in only three models (IPSL-CM5A-MR, CMCC-

339 CESM and IPSL-CM5A-LR) are weaker than the HadISST dataset. Based on the above analysis, it is

340 apparent that the interannual variation of PIOAMI is more closely to IOI than POI, and the interannual

341 variation of PIOAM in autumn can be measured by CCSM4, GISS-E2-R and FGOALS-s2.

342



343

344 **Figure 11: Ratios of standard deviation of autumn IOI, POI and PIOAMI in each model to those in the**  
345 **HadISST dataset. Green bar represents the MME of the corresponding index.**

346

### 347 3.2.3 The relationship of PIOAM with ENSO and IOD

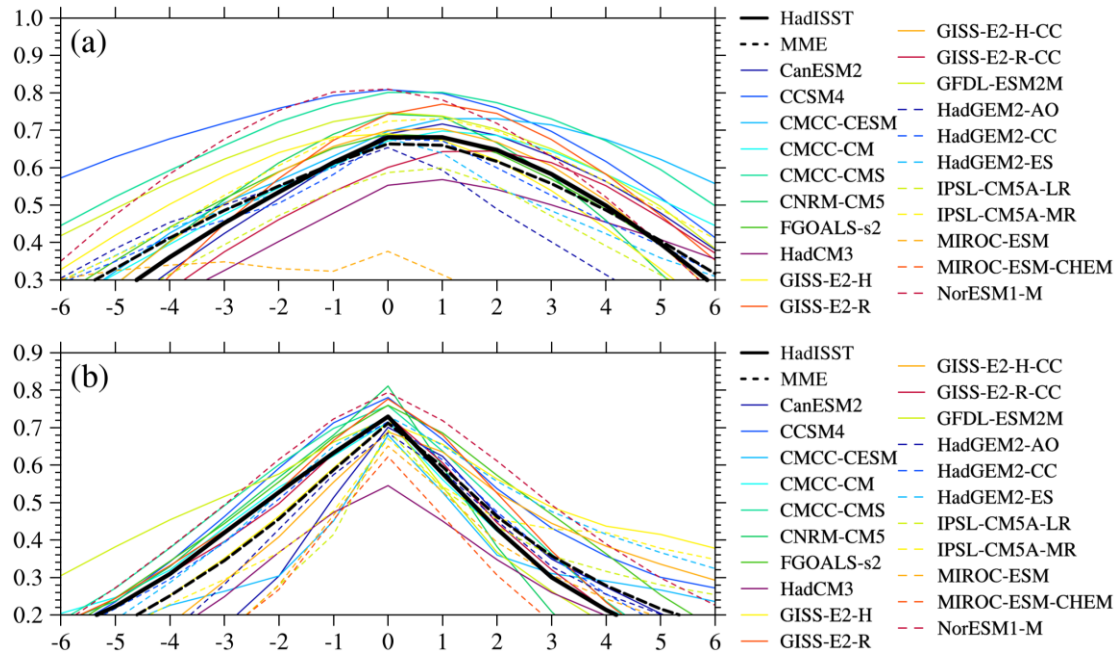


348

349       The lag-lead correlation analysis between PIOAMI and the Niño3.4 index derived from the  
350 HadISST dataset shows that PIOAM has a close correlation with the ENSO mode at the same period and  
351 one month lagging with the correlation coefficient of 0.68 (Fig. 12.a). In addition, PIOAM and IOD also  
352 have a close correlation in the same period, with a correlation coefficient of 0.73 (Fig. 12.b), indicating  
353 that the PIOAM can reflect the activities of ENSO in the Pacific Ocean and IOD in the Indian Ocean to  
354 a considerable extent. It should be noted that the IOD index used in this research is according to the  
355 definition of Saji et al. (1999), i.e. the difference in SSTA between the tropical western Indian Ocean  
356 (50°E-70°E, 10°S-10°N) and the tropical south-eastern Indian Ocean (90°E-110°E, 10°S-0). In these  
357 CMIP5 models, more than one-half of the models successfully reproduce the maximum correlation  
358 between PIOAM and ENSO in the same period. The correlation coefficients of the PIOAMI and the  
359 Niño3.4 index in HadGEM2-AO and HadGEM2-ES are both 0.68, which is consistent with the HadISST  
360 dataset, and the correlation coefficients of FGOALS-s2, GISS-E2-H and GISS-E2-H-CC are 0.69, 0.69  
361 and 0.70, respectively. However, the correlation coefficients of MIROC-ESM and MIROC-ESM-CHEM  
362 are only 0.37 and 0.30, which are significantly different from the results of the HadISST dataset and  
363 other models, indicating that the two models cannot simulate the close relationship between the PIOAM  
364 and ENSO well. In addition, the correlation coefficient of PIOAMI and the Niño3.4 index in MME is  
365 0.66, which is slightly lower than the HadISST dataset but shows the close contemporaneity correlation  
366 between the PIOAM and ENSO; the overall change of the correlation coefficient series is very close to  
367 the HadISST dataset.

368       For the relationship between the PIOAM and IOD, it is apparent from the HadISST dataset in Fig.  
369 12.b that the PIOAM and IOD show obvious close correlation in the same period, and the correlation  
370 coefficient is as high as 0.73. It is satisfactory that all selected CMIP5 models successfully reproduce the  
371 correlation between PIOAM and IOD in the same period, but the simulation results in more than half of  
372 them are underestimated. Among these models, the simulation results of HadGEM2-ES and GIS-E2-R-  
373 CC are basically consistent with the HadISST dataset, which shows that the two models have stronger  
374 capability to simulate the relationship between PIOAM and IOD.

375



376  
 377 **Figure 12: The lag-lead correlation coefficient of the PIOAMI with the Niño3.4 index (a) and IOD index (b).**  
 378 **Ordinate represents the correlation coefficient, and abscissa is the lag in months: positive (negative) for the**  
 379 **Niño3.4 index or IOD index (PIOAMI) leading PIOAMI (Niño3.4 index or IOD index)**

380  
 381 **4. Conclusion and discussion**

382  
 383 Based on HadISST dataset from 1951 to 2005, the Pacific-Indian Ocean associated mode, proposed  
 384 by Yang and Li (2005) is evaluated for 21 CMIP5 models. This research provides a relatively  
 385 comprehensive evaluation of the spatial pattern, the interannual variation and the relationship with ENSO  
 386 and IOD of the PIOAM in the selected CMIP5 models. The main conclusions are as follows.

387 With a 47% contribution to total variance, the spatial pattern of PIOAM in the eastern equatorial  
 388 Pacific Ocean is a warm tongue, whereas there is negative SSTA in the western equatorial Pacific Ocean  
 389 that exhibits an obvious ENSO mode in the Pacific Ocean. In addition, the PIOAM presents an IOD  
 390 mode in the Indian Ocean. The variance contributions of PIOAM in almost all CMIP5 models are smaller  
 391 than that in the HadISST dataset. The simulation errors and differences among these models are mainly  
 392 concentrated in the Pacific Ocean, compared to the Indian Ocean, and a majority of models overestimate  
 393 the strength of PIOAM in the equatorial east Pacific and central Pacific. Although all these models  
 394 reproduce the spatial pattern of the positive SSTA in the eastern equatorial Pacific well, only one-third  
 395 of the models (CCSM4, CMCC-CM, CMCC-CMS, CNRM-CM5, FGOALS-s2, GFDL-ESM2M and  
 396 NorESM1-M) successfully simulate the ENSO mode with the east-west inverse phase in the Pacific

397 Ocean. In general, CCSM4, GFDL-ESM2M and CMCC-CMS have stronger capability to simulate the  
398 PIOAM than the other models.

399 The PIOAM is very weak or not obvious in some years and has obvious seasonal and interannual  
400 variations, as well as interdecadal variations. The simulated strengths of the PIOAM in the positive phase  
401 are underestimated in most models; only less than one-fifth of the models (CCSM4, CMCC-CMS,  
402 CNRM-CM5 and GFDL-ESM2M) are slightly stronger, and very close to the HadISST dataset,  
403 especially CCSM4. The interannual variation of PIOAM in CCSM4, GISS-E2-R and FGOALS-s2 are  
404 almost consistent with the HadISST dataset. Except that NorESM1-M overestimate the interannual  
405 variation of PIOAM, the simulation results in most models are weak, especially MIROC-ESM. The  
406 interannual variation of PIOAM in autumn can be measured by CCSM4, GISS-E2-R and FGOALS-s2.  
407 The PIOAM can well reflect the activities of ENSO in the Pacific Ocean and IOD in the Indian Ocean  
408 to a considerable extent with a close correlation to ENSO and IOD for the same period, as well as one  
409 month in advance with ENSO.

410 It is undoubtedly difficult to directly find the factors that influence the model to simulate  
411 the PIOAM. The simulation results of model families, such as CMCC, IPSL, MIROC, GISS and  
412 HadGEM2, provide clues and comparative data to find the possible reasons that may lead to  
413 simulation differences. However, it needs in-depth analysis which is supported by a large  
414 number of models, or by dedicated experiments.

415 Yang et al. (2006) found that only considering the ENSO in the Pacific cannot entirely  
416 explain the influence of SSTA on climate variation, and suggested that, to provide better  
417 scientific explanation for short-term climate prediction, the PIOAM and its influence should be  
418 considered and investigated. In addition, a review article by Cai et al. (2019) provides the first  
419 comprehensive review and summary of the current research advances in the interaction between  
420 the tropical Pacific-Indo-Atlantic climate systems, and they pointed out that an in-depth  
421 understanding of the dynamic mechanisms of intertropical basin interactions is an important  
422 way to improve the ability of seasonal to decadal climate prediction. Therefore, evaluating and  
423 improving the capability of current climate models to simulate the PIOAM and even the tropical  
424 Pacific-Indo-Atlantic climate systems are beneficial to obtain accurate climate change  
425 predictions. In addition, improving the level of climate prediction is not only helpful to grasp

426 the changes in the ocean environment of the Pacific-Indian Ocean, but also propitious to  
427 improve the ability of prediction and assessment of ocean waves and wind energy (Zheng and  
428 Li, 2015; Zheng and Li, 2017).

429

430 **Data availability.** The CMIP5 data are available at <https://esgf-node.llnl.gov/search/cmip5/>. The sea  
431 surface temperature are available at <https://www.metoffice.gov.uk/hadobs/hadisst/data/download.html>

432

433 **Author contributions.** Xin Li and Weilai Shi conceived the idea and designed the structure of this  
434 paper; Minghao Yang performed the experiments; Minghao Yang, Chao Zhang and Jianqi Zhang  
435 analyzed the data; Minghao Yang wrote the paper.

436

437 **Competing interests.** The author declares that they have no conflict of interest.

438

439 **Acknowledgements.** Two anonymous reviewers provided careful and constructive comments on the  
440 submitted manuscript, which helped improve this article. The first author thanks Handling Topic Editor  
441 David Stevens and Handling Executive Editor John M. Huthnance for their helps to find excellent  
442 reviewers. This research was supported by National Natural Science Foundation of China (4160501,  
443 41490642, 41520104008).

444

445 References:

446

447 Annamalai, H., Xie, S. P., McCreary, J. P. and Murtugudde, R.: Impact of Indian Ocean Sea Surface  
448 Temperature on Developing El Niño. *J. Clim.*, 18(1), 302-319, doi:10.1175/jcli-3268.1, 2005.

449 Bjerknes, J.: A possible response of the atmospheric Hadley circulation to equatorial anomalies of  
450 ocean temperature, *Tellus.*, 18(4), 820-829, doi:10.3402/tellusa.v18i4.9712, 1966.

451 Bjerknes, J.: Atmospheric teleconnections from the equatorial Pacific, *Mon. Wea. Rev.*, 97(3), 163-  
452 172, doi:10.1175/1520-0493(1969)097<0163:atftpe>2.3.co;2, 1969.

453 Cai, W. J., Hendon, H. H. and Meyers, G.: Indian Ocean dipolelike variability in the CSIRO Mark  
454 3 coupled climate model, *J. Climate*, 18(10), 1449-1468, doi: 10.1175/jcli3332.1, 2005.

455 Chen, D., Cane, M. A.: El Niño prediction and predictability, *J. Comput. Phys.*, 227, 3625-3640,  
456 doi: 10.1016/j.jcp.2007.05.014, 2008.

457 Chen, D.: Indo-Pacific Tripole: An intrinsic mode of tropical climate variability, *Adv. Geosci.*, 24,  
458 1-18, doi: 10.1142/9789814355353\_0001, 2011.

459 Cai, W., Wu, L., Lengaigne, M., Li, T., McGregor, Shayne., and et al.: Pan-tropical climate  
460 interactions, *Science*, 363(eaav4236), doi: 10.1126/science.aav4236, 2019.

461 Guo, Y. F., Zhao, Y. and Wang, J.: Numerical simulation of the relationships between the 1998  
462 Yangtze River valley floods and SST anomalies, *Adv Atmos Sci*, 19(3), 391-404,  
463 doi:10.1007/s00376-002-0074-0, 2002.

464 Guo, Y. F.: Numerical simulation of the 1999 Yangtze River valley heavy rainfall including  
465 sensitivity experiments with different anomalies, *Adv Atmos Sci*, 19(3), 391-404, doi:  
466 10.1007/BF02915677, 2004.

467 Huang, B. H. and Kinter, J. L.: Interannual variability in the tropical Indian Ocean, *J. Geophys. Res.*,  
468 107(C11): 3199. doi:10.1029/2001JC001278, 2002.

469 Jin, F. F.: An equatorial ocean recharge paradigm for ENSO. Part I: Conceptual model, *J. Atmos.*  
470 *Sci.*, 54(7), 811-829, doi:10.1175/1520-0469(1997)054<0811:aeorpf>2.0.co;2, 1997.

471 Ju, J. H., Chen, L. L. and Li, C. Y.: The preliminary research of Pacific-Indian Ocean sea surface  
472 temperature anomaly mode and the definition of its index, *Journal of Tropical Meteorology*  
473 (in Chinese), 20(6), 617-624, 2004.

474 Jiang, D. B. and Tian, Z. P.: East Asian monsoon change for the 21st century: results of CMIP3 and  
475 CMIP5 models, *Chinese Science Bulletin*, 58(12), 1427-1435, doi:10.1007/s11434-012-5533-  
476 0, 2012.

477 Klein, S. A. and Soden, B. J.: Remote sea surface temperature variation during ENSO: evidence for  
478 a tropical atmospheric bridge, *J. Clim.*, 12(4), 917-932, doi:10.1175/1520-  
479 0442(1999)012<0917:rsstvd>2.0.co;2, 1999.

480 Li, C. Y. Interaction between anomalous winter monsoon in East Asia and El Niño events, *Adv.*  
481 *Atmos. Sci.*, 7(1), 36-46, doi:10.1007/bf02919166, 1990.

482 Li, C. Y. and Mu, M. Q.: El Niño occurrence and sub-surface ocean temperature anomalies in the  
483 Pacific warm pool, *Chinese Journal of Atmospheric Sciences (in Chinese)*, 23(5), 513-521,  
484 1999.

485 Li, C. Y. and Mu, M. Q.: Relationship between East Asian winter monsoon, warm pool situation and  
486 ENSO cycle, *Chin. Sci. Bull.*, 45(16), 1448-1455, doi:10.1007/BF02898885, 2000.

487 Li, C. Y. and Mu, M. Q.: The influence of the Indian Ocean dipole on atmospheric circulation and  
488 climate. *Adv. Atmos. Sci.*, 18(5), 831-843. doi:10.1007/BF03403506, 2001.

489 Li, C. Y.: A Further Study of the Essence of ENSO, *Climate and Environmental Research* (in  
490 Chinese), 7(2), 160-174, 2002.

491 Li, C. Y., Mu, M. Q., and Pan, J.: Indian Ocean temperature dipole and SSTA in the equatorial  
492 Pacific Ocean, *Chin. Sci. Bull.*, 47(3), 236-239, doi:10.1360/02tb9056, 2002.

493 Li, T., Wang, B., Chang, C. P. and Zhang, Y.: A theory for the Indian Ocean dipole-zonal mode, *J.*  
494 *Atmos. Sci.*, 60(17): 2119-2135, doi: 10.1175/1520-0469(2003)060<2119:atftio>2.0.co;2,  
495 2003.

496 Li, C. Y., Mu, M., Zhou, G. Q. and Yang, H.: Mechanism and prediction studies of the ENSO,  
497 *Chinese Journal of Atmospheric Sciences* (in Chinese), 32(4), 761-781, 2008.

498 Liu, H., Lin, P., Yu, Y. and Zhang, X.: The baseline evaluation of LASG/IAP Climate system Ocean  
499 Model (LICOM) version 2, *Acta. Meteor. Sin.*, 26(3), 318-329, doi:10.1007/s13351-012-0305-  
500 y, 2012.

501 Lian, T., Chen, D. K., Tang, Y. M., Jin, B. G.: A theoretical investigation of the tropical Indo-Pacific  
502 tripole mode, *Sci. China-Earth Sci.*, 57, 174-188, doi: 10.1007/s11430-013-4762-7, 2014.

503 Li, X. and Li, C. Y.: The tropical pacific–indian ocean associated mode simulated by licom2.0, *Adv.*  
504 *Atmos. Sci.*, 34(12), 1426-1436, doi:10.1007/s00376-017-6176-5, 2017.

505 Li, C. Y., Li, X., Yang, H., Pan, J. and Li, G.: Tropical Pacific-Indian Ocean Associated Mode and  
506 Its Climatic Impacts *Chinese Journal of Atmospheric Sciences* (in Chinese), 42(3), 505-523,  
507 2018.

508 Mu, M. and Duan, W. S.: A new approach to studying ENSO predictability: Conditional nonlinear  
509 optimal perturbation, *Chin. Sci. Bull.*, 48(10), 1045-1047, doi:10.1007/BF03184224, 2003.

510 Mu, M., Duan, W. S. and Wang, B.: Season-dependent dynamics of nonlinear optimal error growth  
511 and El Niño-Southern Oscillation predictability in a theoretical model, *Journal of Geophysical*  
512 *Research: Atmospheres*, 112(D10), doi:10.1029/2005JD006981, 2007.

513 North G. R., Bell, T. L., Cahalan, R. F., Moeng, F. J.: Sampling errors in the estimation of empirical  
514 orthogonal functions, *Mon. Wea. Rev.*, 110, 699-706, doi: 10.1175/1520-  
515 0493(1982)110<0699:seiteo>2.0.co;2, 1982.

516 Philander, S. G. H., Yamagata, T. and Pacanowski, R. C.: Unstable Air-Sea Interactions in the  
517 Tropics, *J. Atmos. Sci.*, 41(4), 604-613, doi: 10.1175/1520-  
518 0469(1984)041<0604:UASIIT>2.0.CO;2, 1984.

519 Rasmusson, E. M. and Wallace, J. M.: Meteorological aspects of the El Niño/Southern Oscillation,  
520 *Science*, 222(4629), 1195-1202, doi:10.1126/science.222.4629.1195, 1983.

521 Ropelewski, C. F. and Halpert, M. S.: Global and regional scale precipitation patterns associated  
522 with the El Niño/southern Oscillation, *Mon. Wea. Rev.*, 115(8), 1606-1626, doi:10.1175/1520-  
523 0493(1987)115.0.CO;2, 1987.

524 Rayner, N. A., Parker, D. E., Horton, E. B., Folland, C. K., Alexander, L. V., Rowell, D. P., Kent, E.  
525 C. and Kaplan, A.: Global analyses of sea surface temperature, sea ice, and night marine air  
526 temperature since the late nineteenth century, *J. Geophys. Res.*, 108(D14), 4407  
527 doi:10.1029/2002JD002670, 2003.

528 Rao, S. A., Masson, S., Luo, J. J., Behera, S. K. and Yamagata, T.: Termination of indian ocean  
529 dipole events in a coupled general circulation model, *J. Climate*, 20(13), 3018-3035,  
530 doi:10.1175/JCLI4164.1, 2007.

531 Suarez, M. J. and Schopf, P. S.: A delayed action oscillator for ENSO, *J. Atmos. Sci.*, 45(21), 3283-  
532 3287, doi: 10.1175/1520-0469(1988)045<3283:adaofe>2.0.co;2, 1988.

533 Saji, N. H., Coswami, B. N., Vinayachandran, P. N. and Yamagata, T.: A dipole in the tropical Indian  
534 Ocean, *Nature*, 401(6751), 360-363, doi:10.1038/43854, 1999.

535 Shen, X. S., Kimoto, M., Sumi, A., Numaguti, A. and Matsumoto, Jun.: Simulation of the 1998 East  
536 Asian Summer Monsoon by the CCSR/NIES AGCM. *J Meteor Soc Japan*, 79(3), 741-757,  
537 doi:10.2151/jmsj.79.741, 2001.

538 Saji, N. H. and Yamagata, T.: Possible impacts of Indian Ocean dipole mode events on global climate,  
539 *Climate Research*, 25(2), 151-169, doi: 10.3354/cr025151, 2003.

540 Taylor, K. E.: Summarizing multiple aspects of model performance in a single diagram, *Journal of*  
541 *Geophysical Research: Atmospheres*, 106(D7), 7183-7192, doi:10.1029/2000jd900719, 2001.

542 Ueda, H. and Matsumoto, J.: A possible triggering process of East–West asymmetric anomalies over  
543 the Indian Ocean in relation to 1997/98 El Niño, *J. Meteor. Soc. Japan*, 78(6), 803-818,  
544 doi:10.2151/jmsj1965.78.6\_803, 2000.

545 Wyrтки, K.: El Niño-The Dynamic Response of the Equatorial Pacific Ocean to Atmospheric Forcing,  
546 *J. Phys. Oceanogr.*, 5(4), 572-584, doi:10.1175/1520-0485(1975)005<0572:entdro>2.0.co;2,  
547 1975.

548 Webster, P. J. and Yang, S.: Monsoon and ENSO: Selectively interactive systems. *Quart. J. Roy.*  
549 *Meteor. Soc.*, 118(507), 877-926, doi:10.1002/qj.49711850705, 1992.

550 Webster, P. J., Moore, A. M., Loschnigg, J. P. and Leben R. R.: Coupled ocean-atmosphere dynamics  
551 in the Indian Ocean during 1997-98, *Nature*, 401(6751), 356-360, doi: 10.1038/43848, 1999.

552 Wang, X. and Wang, C. Z.: Different impacts of various El Niño events on the Indian Ocean Dipole,  
553 *Climate Dyn.*, 42(3-4), 991-1005, doi: 10.1175/JCLI-D-12-00638.1, 2014.

554 Yu, L. S. and Rienecker, M. M.: Mechanisms for the Indian Ocean warming during the 1997-98 El  
555 Niño, *Geophys. Res. Lett.*, 26(6), 735-738, doi:10.1029/1999GL900072, 1999.

556 Yang, H. and Li, C. Y.: Effect of the Tropical Pacific-Indian Ocean Temperature Anomaly Mode on  
557 the South Asia High, *Chinese Journal of Atmospheric Science (in Chinese)*, 29(1): 99-110,  
558 2005.

559 Yang, H., Jia, X. L. and Li, C. Y.: The tropical Pacific-Indian Ocean temperature anomaly mode and  
560 its effect, *Chin. Sci. Bull.*, 51(23): 2878-2884, doi:10.1007/s11434-006-2199-5, 2006.

561 Yang, M., Li, X., Zuo, R., Chen, X. and Wang, L.: Climatology and Interannual Variability of Winter  
562 North Pacific Storm Track in CMIP5 Models, *Atmosphere*, 9(3), 79,  
563 doi:10.3390/atmos9030079, 2018.

564 Zhou, G. Q. and Zeng, Q. C.: Predictions of ENSO with a coupled atmosphere–ocean general  
565 circulation model, *Adv. Atmos. Sci.*, 18(4), 587-603, doi:10.1007/s00376-001-0047-8, 2001.

566 Zheng, F., Zhu, J. and Zhang, R. H.: The impact of altimetry data on ENSO ensemble initializations  
567 and predictions, *Geophys. Res. Lett.*, 34(13), doi:10.1029/2007gl030451, 2007.

568 Zheng, X. T., Xie, S. P., Du, Y., Liu, L., Huang, G. and Liu, Q.: Indian Ocean Dipole Response to  
569 Global Warming in the CMIP5 Multimodel Ensemble, *J. Climate*, 26(16), doi:6067-6080,  
570 10.1175/JCLI-D-12-00638.1, 2013.

571 Zheng, C. W. and Li, C. Y.: Variation of the wave energy and significant wave height in the China  
572 Sea and adjacent waters. *Renewable and Sustainable Energy Reviews*, 43, 381-387,  
573 doi:10.1016/j.rser.2014.11.001, 2015.

574 Zheng, C. W. and Li, C. Y.: Propagation characteristic and intraseasonal oscillation of the swell  
575 energy of the Indian Ocean, *Applied Energy*, 197, 342-353,  
576 doi:10.1016/j.apenergy.2017.04.052, 2017.